ACS Photonics

Article

pubs.acs.org/journal/apchd5

High-Speed, High-Sensitivity Optoelectronic Device with Bilayer Electron and Hole Charge Plasma

Bahram Nabet,*[,†] Marc Currie,[‡] Pouya Dianat,[†] Fabio Quaranta,[§,⊥] and Adriano Cola[§,⊥]

[†]Electrical and Computer Engineering Department, Drexel University, Philadelphia, Pennsylvania 19038, United States

[‡]Optical Sciences Division, Naval Research Laboratory, Washington, D.C. 20375, United States

[§]IMM-CNR, Institute for Microelectronics and Microsystems, Unit of Lecce, National Research Council, Via Monteroni, Lecce I-73100, Italy

ABSTRACT: Analogous to a drop exciting a wave in a reservoir that is detected more rapidly than the drop's transport by current flow, charge plasma confined in a semiconductor can transfer energy, hence respond much faster than the electric field-induced carrier drift current. Here we construct an optoelectronic device in which charge reservoirs respond to excitation with a speed that is impossible to achieve by transport of charge. In response to short optical pulses, this device produces electrical pulses that are almost 2 orders of magnitude shorter than the same device without the charge reservoirs. In addition to speed, the sensitivity of this process allowed us to measure, at room temperature, as low as 11 000 photons. These micro plasma devices can have a range of applications such as optical communication with a fraction of a microwatt power compared to the present tens of milliwatts, ultrasensitive light detection without cryogenic cooling, photovoltaic devices capable of harvesting dim light, THz radiation detectors, and charged particle detectors.

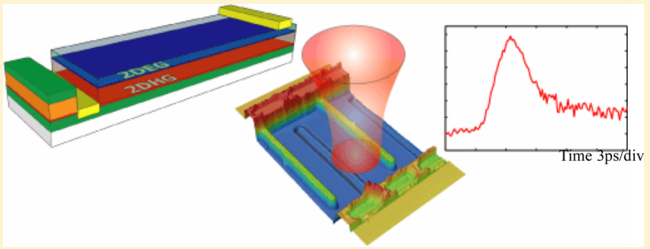

KEYWORDS: *two-dimensional gas, charge plasma, charge transport, dispersion relation, E−K relation, photodetectors*

Two perspectives have historically defined electronics: one is based on the transport of charged particles and the other on the transport of a wave in a medium of charge carriers. The former is the transport of (discrete) charge carriers whose velocity then results from their acceleration by the force of the electric field and is the foundation of transistor-based microelectronics.[1,2] This velocity is derived from electrons' energy-momentum ($E-K$) relation and is about 10^7 cm/s in high-mobility semiconductors such as GaAs. Electron and hole effective masses are also derived from the $E-K$ relation as an important particle-like characteristic of these charge carriers. In contrast, wave motion is built upon a dielectric function, $\varepsilon(\omega)$, that characterizes the collective response of a medium to electric field excitation. The wave motion in a medium with $\varepsilon(\omega)$ can be derived from Maxwell's equations, and a dispersion relation ($\omega-K$) can be found, from which, similar to the $E-K$ relation, information about the group velocity of the wave traveling in the medium can be extracted. This wave (group) velocity is well over an order of magnitude higher than the electron velocity caused by the force of the electric field[3] and may be considered the basis of electronics as envisioned by Langmuir,[4] Debye,[5] Bohm,[6] Gabor,[7] and Landau,[8] among others.

The wave motion in an electron gas medium has time constants on the order of the dielectric relaxation time of the medium—proportional to the product of the medium's permittivity ε_s and resistivity ρ—which for high charge densities is in the tens of femtoseconds range, while time constants based on charged particle motion are much slower.[3] This is to be expected since the former can be an energy relaxation process, while the latter is due to real charge motion caused by carrier acceleration due to the force of the electric field and deceleration due to scattering. By analogy, if electron transport current is similar to water flow in a river, the dielectric response is the wave in a pond. In this report we use the collective response of two-dimensional electron and hole gas reservoirs in a semiconductor to (optical) excitation in order to achieve speed and sensitivity beyond what is possible to obtain when charge transport is necessary. These reservoirs of charge are composed of sheets of electrons and holes whose motion is confined to two dimensions rather than the 3D motion that occurs in bulk semiconductors. The study of the interaction of electromagnetic radiation with structures that confine electrons to an interface, such as metals, was pioneered in 1957,[9] and verification of the collective modes of electron excitation, plasmons, appeared in 1960.[10] Besides metals, collective properties of electron gases such as at dielectric interfaces, or the surface of liquid helium, have been the subject of intense interest.[11] This was motivated by the study of the surface states in metal−insulator−semiconductor devices[2] and in the silicon metal oxide semiconductor field effect transistor (MOSFET) device.[12] Collective modes of excitations, plasmons, in a two-dimensional electron gas (2DEG) were first observed in electrons trapped by the image potential on the surface of liquid helium in 1976[13] and then in the inversion layer of a MOSFET.[12]

Received: November 14, 2013

   dx.doi.org/10.1021/ph4001229 | *ACS Photonics* XXXX, XXX, XXX−XXX

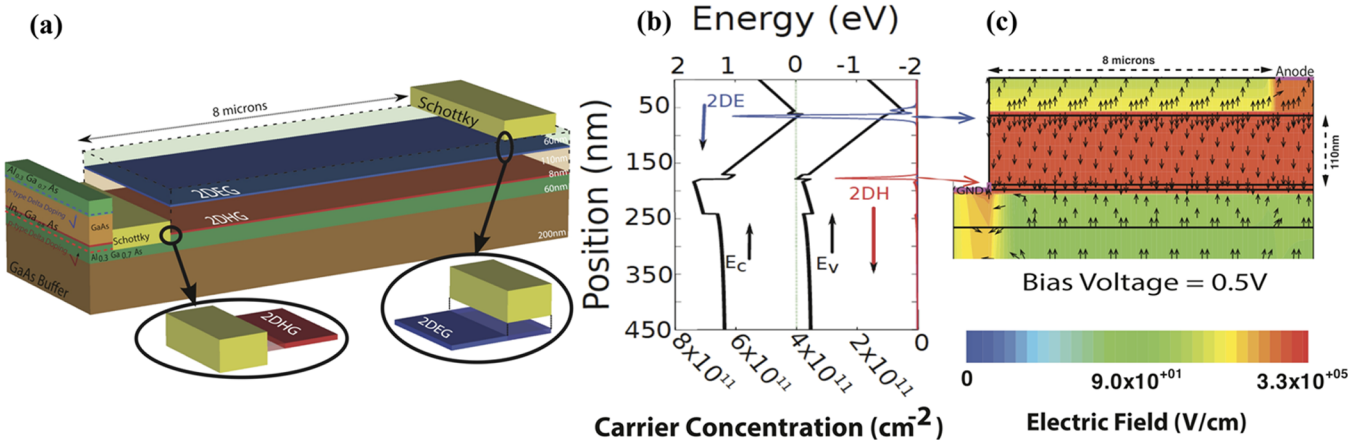

Figure 1. (a) Schematic of the device layer structure with two reservoirs of two-dimensional electron and hole gases separated by a ~110 nm region that absorbs light. Blocking Schottky contacts form the cathode and anode that are >8 μm apart and separately contact sheets of charge. (b) Calculated energy band diagram along the direction of growth in the middle of the device showing the existence of a large vertical electric field, as well as dense electron (6×10^{11} cm^{-2}) and hole (3×10^{11} cm^{-2}) gases which can move in only two dimensions. (c) Simulation showing a large vertical field (>100 kV/cm) in the region between the electron and hole 2D charge reservoirs under 0.5 V applied bias. Horizontal and vertical length scales are different.

Direct interaction of radiation with the electrons in the MOSFET inversion channel was studied as early as 1976.[14] Serious interest in the room-temperature properties of the 2DEG began on the "inversion channel" of AlGaAs/GaAs heterojunctions[15] and on InP.[16] Though initiated for the study of the collective behavior of the electron plasma, the reduced electron scattering and higher mobility of the 2DEG compared to the bulk resulted in its successful incorporation as the charge transport channel of high electron mobility (HEMT) transistors.[17−19] Presently such transistors hold the highest speed of operation record at well over 650 GHz,[20] which is primarily limited by the transport time of electrons in the <40 nm distance between the source and the drain electrodes. Hydrodynamic modeling of the 2DEG as a whole[21] has shown the possibility of plasma wave propagation, and hence much higher speed of operation, in HEMTs with lengths less than momentum relaxation distance. This has resulted in a range of plasma wave electronic devices.[22]

Here we present an optoelectronic device with bilayer reservoirs of confined electrons and holes, with contact separation as large as 8.5 μm, much larger than momentum relaxation distance. In response to a 400 fs perturbation by as little as ~11 000 photons, this device produced a short, less than 2.5 ps, electric pulse, which would take over 100 ps if it were based on charge transport. This device shares some features with the metal−semiconductor−metal (MSM) photodetectors, PIN photodiodes, and waveguide photodetectors, which constitute state-of-the-art high-speed photodetectors,[23−25] but is distinct from them and competes favorably in terms of speed, sensitivity, and power as detailed below. The physics of the device operation and applications of such microplasma-based devices will also be discussed.

RESULTS AND DISCUSSION

Figure 1 shows the device layer structure that produced confined 2DEG and two-dimensional hole gas (2DHG). The wafer was grown by metal organic chemical vapor deposition (MOCVD) on semi-insulating GaAs. After growth of a buffer layer, 57 nm of $Al_{0.3}Ga_{0.7}As$ was lattice-match grown and delta-doped (p-type) with carbon at 2.5×10^{12} cm^{-2}. A spacer layer of AlGaAs then made a heterojunction with an 8 nm layer of the (strained) narrow band gap $In_{0.2}Ga_{0.8}As$. The valence band offset keeps the hole gas, produced by the acceptor dopants, from moving in the direction of growth, but the carriers are free to move in the other two dimensions, thus forming a 2DHG. A 109.4 nm layer of GaAs was then grown on top of the InGaAs layer in order to absorb light and excite the 2D reservoirs with optically generated carriers. This was followed by a 5 nm AlGaAs spacer and a 56.4 nm AlGaAs n-type layer delta-doped with Si at 6×10^{12} cm^{-2} that produced a 2D electron gas at this interface. The energy band diagram (EBD) of this structure was calculated by self-consistent solution of Poisson and Schrodinger equations and is shown in Figure 1b. Electron and hole distributions were also calculated and shown. These indicate the existence of relatively dense concentrations, ~6.5×10^{11} cm^{-2} electrons and ~2.2×10^{11} cm^{-2} holes, and are verified by Hall measurements. The electric field profile under an applied bias of 0.5 V was calculated, using the Synopsys Sentaurus simulation package, and is shown in Figure 1c. Since the gradient of the EBD is the electric field, both parts a and b in Figure 1 show a large vertical field (>100 kV/cm) in the direction of growth. Detailed simulations supported by capacitance−voltage measurements show the horizontal component of the electric field is due to the applied bias and is shielded by the charge reservoirs, which remain intact for small biases. This produces equipotential surfaces, which terminate electric field lines.[26] Several device geometries were fabricated with varying distances between contacts, interdigitation, contact depths, transmission line incorporation, and passivation. Additionally, geometrically identical devices were fabricated for comparison purposes. These either had a single 2DEG or 2DHG layer or were undoped conventional structures without the two-dimensional reservoirs of charge. In addition, some wafers had Bragg layers in a resonant cavity enhanced (RCE) structure. Details are provided in the Methods section. An image of the fabricated device is shown in Figure 2, with a cross-sectional cut demonstrating that the 2DEG and 2DHG are separately contacted by evaporation of metals, which formed blocking Schottky contacts. The interdigitated contacts were asymmetrically spaced 8.2 and 8.7 μm apart, although a number of devices with various contact separations were fabricated for comparison. Fabrication details are also provided in the Methods section.

This device is similar to the planar metal−semiconductor−metal[23] photodetectors in the in-plane direction. In addition, due to its 2DH−insulator−2DE vertical structure, it is similar to a

dx.doi.org/10.1021/ph4001229 | ACS Photonics XXXX, XXX, XXX−XXX

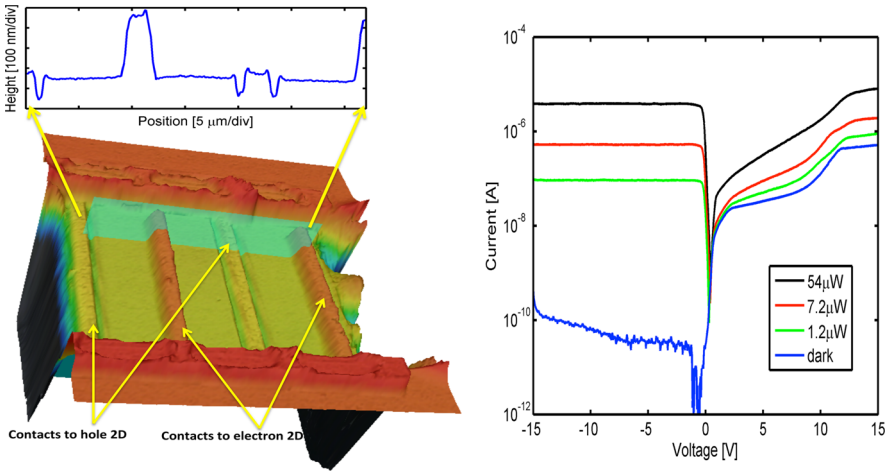

Figure 2. (Left) Image of the fabricated device. Rectifying (Schottky) contacts are made separately to two-dimensional electron and hole reservoirs. Contact separations are over 8 μm as the cross-sectional cut above the figure shows. (Right) Current−voltage measurements in ambient light and under 1.2, 7.2, and 54 μW of optical power, respectively, showing only a small amount of current that flows in the dark despite high concentrations of charge.

PIN photodiode in the direction of growth. It also has similarities to waveguide and traveling wave photodetectors (WGPD, TWPD), with the 2D charge plasma sheets replacing the metal waveguides.[24,25] It is, however, distinct from these devices in crucial characteristics. It is not the vertical PIN where the ohmic contacts (to p+ and n+ doped regions) are separated by the thin intrinsic absorption region. It has the planar simplicity of top-illuminated MSM but not the electric field landscape that sweeps the carriers to be collected at the Schottky contacts that are >8 μm apart. Instead there exists a strong (>100 kV/cm) vertical field that separates the 2D charge reservoirs. Carrier motion is to these reservoirs, whose collective response produces the electric signal at the contacts, and, contrary to the side-illuminated WGPD and TWPDs, it does not need (long) metallic transmission lines, although it offers the same speed of response. An interesting, somewhat similar, structure consisting of double graphene layers has recently been proposed for resonant excitation of plasma oscillations.[27] Similar electron−hole bilayer systems have been investigated in a different context since the prediction of formation of bound electron−hole excitons[28] in parallel sheets of electrons and holes by Keldysh in 1968. This could result in important anomalous behavior such as the formation of Bose−Einstein condensates or possibly super-solids.[29] However, these properties are expected to occur when the layers are much closer than the typical interparticle distance of a few nanometers,[30,31] which is not the case in our structures.

The current−voltage (I−V) measurements in ambient room light (dark) and under continuous wave (CW) illumination by an 830 nm Ti:sapphire laser at three different optical intensity levels are also shown in Figure 2. The dark I−V is asymmetric due to differences in the contact between the metal and the 2D electron and hole gases. This produces currents below 100 pA when the contact to 2DHG is the cathode and remains under 50 nA when the 2DEG contact is the cathode. This is expected since the dark current is due to thermionic emission, i.e., due to electrons, or holes, that have sufficient kinetic (thermal) energy to overcome the potential barrier between the metal and the semiconductor. This thermionic emission current is modified when the semiconductor is two-dimensional since the barrier height is increased by the confined energy levels of the semiconductor, as well as by the repulsive effect of the 2D charges on the carriers that are emitted from the metal.[32] The very low dark currents observed here signify that the blocking contacts maintain the confined reservoirs of charge under quasi-equilibrium, with a small amount of current flowing by thermionic emission. Had these contacts been ohmic, as is the case for the source and the drain of a transistor, up to 8 orders[19] of magnitude more current, in the tens of mA range, would be expected to flow, given the contact areas and the density of electron and hole gases.

The device is illuminated with an 830 nm wavelength laser that is absorbed in the ∼110 nm thick GaAs layer. This absorption layer is sandwiched between two-dimensional sheets of electron and hole gas reservoirs. Without the 2DEG and 2DHG reservoirs the photogenerated carriers would be swept by the lateral electric field between the Schottky contacts and collected at the contacts. Here, however, as the simulation of the electric field in Figure 1c and the slope of the energy band diagram in Figure 1b show, there is a vertical electric field of >100 kV/cm that moves the optically generated electrons to the (top) 2DEG and holes to the (bottom) 2DHG. These optically generated carriers perturb the charge reservoirs, eliciting a collective response that is not limited by the transit of the charges to the contacts. The I−V response in Figure 2 shows that the device is an efficient optical detector with 5 orders of magnitude current change caused by a 54 μW optical excitation. This dc responsivity, corrected for reflection from the AlGaAs surface, is 0.12 A/W. At 830 nm, the maximum responsivity of bulk GaAs with 100% internal quantum efficiency (accounting for ∼30% reflectivity from the AlGaAs surface) is 0.47 A/W; however, for a thickness of d = 110 nm and absorption coefficient $\alpha = 10^4$ cm^{-1}, $(1 - \exp(-\alpha d)) = 9.5\%$ of incident photons are absorbed. Our dc responsivity is thus ∼2.5 times the maximum responsivity expected from a 110 nm thick absorption region and is mostly due to the collection of carriers generated outside this thin region, which are efficiently collected in the 2DE, 2DH reservoirs. The device is also very sensitive, with 1.2 μW of light causing a current change by a factor of over 4000 compared to the device in the dark and as low as 1.2 nW being detectable. The dc light responsivity and sensitivity are, however, secondary to the dynamic behavior of this device, as we discuss next.

The dynamic response is probed by exciting the device with short, 400 fs, pulses of light generated by a Ti:sapphire laser with a center wavelength tunable from 750 to 1080 nm. Absorption of these pulses generates electron and hole pairs in

dx.doi.org/10.1021/ph4001229 | ACS Photonics XXXX, XXX, XXX−XXX

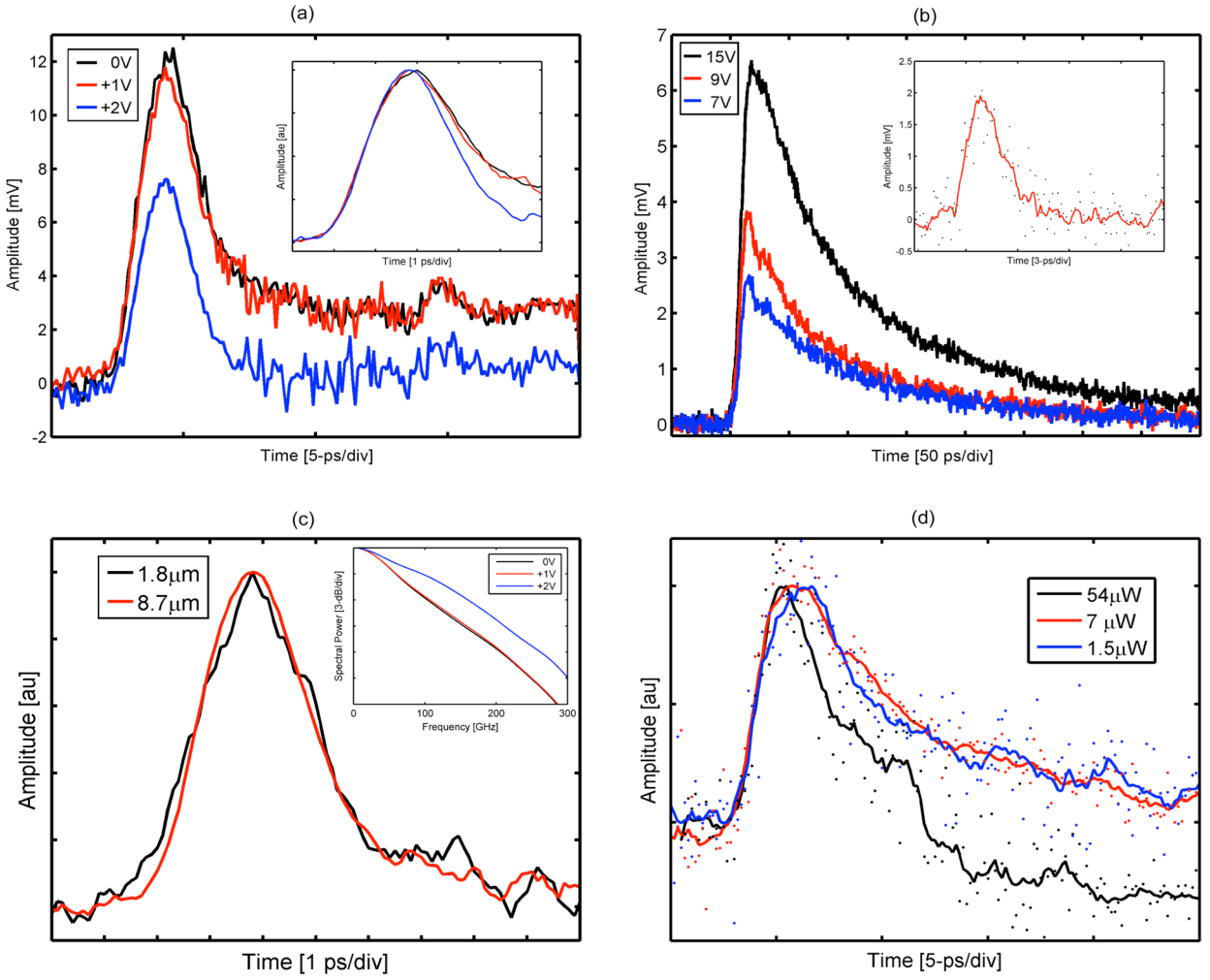

Figure 3. (a) Time response to ∼400 fs light pulses with 54 μW optical power, at 0 (black), 1 (red), and 2 (blue) V bias. Inset is normalized to the peak showing 2.9, 2.9, and 2.5 ps full-width at half-max (fwhm) pulse width, respectively, for the device with >8.5 μm distance between the cathode and anode. (b) Time response of a device with a 8.5 μm gap distance, but without 2D electron and 2D hole reservoirs, under 7 (blue), 9 (red), and 15 (black) V bias showing a fwhm of 50, 55, and 75 ps, respectively, limited by electron transit time, with a 200−250 ps tail that is due to the slow moving holes. Inset is time response of a device with similar geometry under the same optical power; it is much faster with <2.9 fwhm and ∼2 ps fall time, due to the collective 2DEG, and 2DHG response. (c) Time responses for devices with 1.8 and 8.7 μm transit distances are nearly identical and are independent of charge transport distance. Inset is the Fourier Transform of time response under 0,1, and 2 V bias, respectively. (d) Measured time response at various optical powers under 2 V bias showing high sensitivity: at the lowest power, nearly 10 500 photons that are absorbed in the GaAs region produce the electric pulse consisting of ∼1500 electrons. All experiments were at room temperature.

the (∼110 nm thick) GaAs region. Subject to the large vertical electric field, electrons and holes separate and drift, respectively, toward the 2DEG and 2DHG reservoirs, which laterally extend the long (>8 μm) distance between the contacts. High-speed testing is performed with an electro-optic sampling (EOS) system, described in the Methods section of the paper, which can be simply thought of as an ultrafast sampling oscilloscope that uses 400 fs laser pulses to excite optoelectronic transients and then measures the electronic response by probing the refractive index change of an electro-optic crystal (e.g, $LiTaO_3$) placed on top of the device. For our experiment, the device's electronic response is coupled to a coplanar strip (CPS) transmission line; the separation from the excitation fiber to the optical sampling crystal is 250 μm. Since the electro-optic crystal is sensitive to electric field (rather than voltage), sampling near the device could also probe local electric field variations, which can mask the propagating signal. Sampling the electric field 250 μm away on the CPS transmission line removes the local field effects, but also attenuates and disperses the sub-THz propagating pulse.

The measured time responses to the optical ∼400 fs pulses with 54 μW optical average power and applied biases of 0, 1, and 2 V are shown in Figure 3a. The same data normalized to peak values are shown in the inset of the figure. The pulses have a relatively symmetrical shape with similar rise and fall times, with full-width at half-maximum (fwhm) pulse widths of 2.9, 2.9, and 2.4 ps, respectively. The 1.4 ps rise time of the response is longer than our EOS system response and is potentially due to transmission line dispersion occurring from the electrical pulse's 250 μm propagation distance. This would suggest an even faster intrinsic device response conservatively estimated to be about 0.4 ps less than the measured values. This short response cannot be due to the transit of electrons to the anode, which, in the best case of saturation drift velocity of 10^7 cm/s, would be around 80 ps, with holes taking nearly 10 times longer to reach the cathode, depending on the electric field intensity. The peak amplitude of the response with 2 V applied bias is lower than the 0 and 1 V biases; however, the pulse returns to zero level in this case with a shorter (2.4 ps) fwhm value and has a similar max-to-min

dx.doi.org/10.1021/ph4001229 | ACS Photonics XXXX, XXX, XXX−XXX

value (~8 mV). While we do not fully understand the reason for this behavior, simulations show depletion of charge, and screening of the vertical field by the applied bias may account for the decrease in amplitude. The time response of a similar device with 8 μm contact separation of contacts but without the charge reservoirs is shown in Figure 3b. The temporal pulse width for 11 μW incident power measures 50, 55, and 75 ps (fwhm) for respectively 7, 9, and 15 V applied bias. The larger biases were chosen to ensure carrier sweep out for a meaningful comparison. The response tail, i.e., the fall time, which depends on the transport and collection of slow moving carriers, is as long as 200−250 ps in this device. This may be contrasted with the 3 ps (fwhm) response with a <2 ps fall time shown in the inset of Figure 3b for a device with 2DEG and 2DHG reservoirs under 7 μW of power and a more than 8.2 μm cathode−anode distance. The orders-of-magnitude increase in speed is mediated by the collective response of the charge reservoirs that circumvent drift velocity limitations. The short response tail shows that holes are "collected" with the same efficacy as the electrons. That is, the single carrier momentum $m^*\nu = \hbar k$, where m^* is the effective mass, does not limit the response; rather, the time constants depend on the collective response of the hole plasma.

Further indication that the response is not due to the transport of charge carriers to the contacts is provided by comparing the response of two devices with gap distances of 1.8 and 8.7 μm, respectively, in Figure 3c. The response of the device with nearly 5 times the gap distance is practically identical to the shorter one, not only in rise time and pulse width but also in fall time. This also supports the argument that the 2D hole reservoir reacts in the same manner as the 2D electron reservoir with time constants that are on the order of dielectric relaxation time, implying that the hole effective mass (used to determine the drift velocity in response to the electric field's force in the $E-K$ relation) is rather immaterial. Here transfer of energy occurs due to the collective response of the medium. Additionally, the response was observed to be independent of the spatial location of a 1 μm wide beam; that is, the fast speed is not due to carriers collected near one contact.

As previously noted, the key to device operation is that the dense charge plasma is maintained in quasi-equilibrium by using blocking Schottky contacts and applying relatively small biases. If a large bias is applied or if perturbation by light produces a large number of carriers, device performance degrades. In fact, the device can operate at zero electric bias as shown in Figure 3a. This may be explained by observing that after the photogenerated electrons and holes reach their 2DEG and 2DHG reservoirs, respectively, a potential difference and separation of the quasi Fermi levels is created, thereby launching the electric signal onto the transmission line. This is evident if the device is viewed in the vertical direction as 2DHG−intrinsic−2DEG, similar to a PIN photodetector, which has well-known photovoltaic properties, and where current flows under zero bias. The inset in Figure 3c is the Fourier transform of the measured time response at 0, 1, and 2 V of bias, showing that this device operates at hundreds of gigahertz as a photodetector with only a fraction of a microwatt of optical power and no need for voltage bias.

High sensitivity is expected from the picture of a reservoir perturbed by a small excitation, similar to observing the ripples caused by a drop of water on a serene lake. Response to ~400 fs pulses with 1.5, 7, and 54 μW of average optical power under 2 V bias, shown in Figure 3d, corroborates with this expectation. The 1.5 μW light pulse of 400 fs duration, repeated at 76 MHz and chopped at 50% duty cycle, corresponds to roughly 4×10^{-14} Joules of energy, or equivalently, 167 000 photons at a wavelength of 830 nm. Considering 30% reflectivity from the AlGaAs surface and 10% reflection by the metal electrodes, this corresponds to an incident flux of 105 000 photons. Moreover, given the absorption coefficient of GaAs, nearly 90% of these photons penetrate through the ~110 nm thick GaAs absorption layer without being absorbed. At such low flux, photon absorption is probabilistic. Furthermore, the generated electron hole pairs (EHPs) move to charge reservoirs and will scatter and recombine. The third source of loss is the charge density wave loss in the >8 μm long 2D reservoirs. Lastly, the microwave signal travels 250 μm on the transmission line from the device to the probes, suffering its associated losses. Nevertheless, the 10 500 photons in the absorption region produce a 6.5 ps wide and 1.5 mV tall pulse with an identical pulse propagating in each half of the 80 ohm transmission line, resulting in $N = I \times \mathrm{d}t/q$ = 1500 electrons per pulse. This is remarkable considering that the device operates at room temperature, while such levels are typically expected from cryogenically operated detectors.

The data show that the collective response of the plasma overcomes charge transport limitations; however the exact mechanism of the response of the device needs to be further discussed. We follow a two-step process to analyze device dynamics. First, the effect of the motion of optically generated carriers to charge reservoirs under the force of the electric field, shown in Figure 1c, is calculated using the Shockley−Ramo model,[33,34] which was originally proposed for one dimension, but a two-dimensional model can be derived by equating the work done by the motion of the charge $(-q\vec{E}\,\mathrm{d}x)$ with the energy provided by the external circuit $(i(t)V\,\mathrm{d}t)$. This allows evaluation of the current induced in the external circuit as[35]

$$J_{\mathrm{ph}} = \sum_{q} q\vec{\nu}(\vec{r})\,\vec{E}(\vec{r})/V$$

where, $\vec{v}(\vec{r})$ is the velocity of a moving carrier, $\vec{E}$ is the component in the direction $\vec{\nu}$ of the electric field, which exists at the electron's instantaneous position, and V is the applied bias. The total induced current can be calculated by summing over all the charges, namely, electrons and holes, in the active region. The equation involves the usual assumptions that induced currents due to magnetic effects are negligible but incorporate the displacement current since it self-consistently accounts for the electric field perturbation. Simulations start by depositing optically generated carriers in a mesh in which the electric field values are as calculated in Figure 1c. Motion of charge particles instantaneously produces current in the external circuit, with integral of $i(t)$ being one unit of charge when EHPs reach their respective contacts, i.e., are collected, which in this case are the 2DE and 2DH reservoirs. Consequently, the limiting factor in device speed is the transit of electrons and holes in the short ~110 nm thick absorption layer, since energy transfer in the long (>8.5) μm charge reservoirs takes significantly shorter time. Typical trade-off between absorption region thickness and response speed exist and can be improved by multilayers of 2DE/2DH structures, resonant cavity structures,[35] or plasmonic light-trapping structures, which increase the optical path length.[36]

Once the carriers reach the reservoirs, they cause charge imbalance, hence an internal field, resulting in a redistribution of charge and a dielectric relaxation. The relaxation time is calculated from solution of Poisson's equation and is proportional to the dielectric constant ε_s and inversely proportional to the charge density. This dielectric relaxation time is in the range of a few femtoseconds in our case. We model this process of the perturbation of charge reservoirs by the ensemble Monte Carlo (EMC) technique.[37] We start by considering the scattering rate

dx.doi.org/10.1021/ph4001229 | ACS Photonics XXXX, XXX, XXX−XXX

between an electron in the 2D well with wave vector k in subband i and a second electron with wave vector k_0 in the subband j. The final states of these two electrons are k_0 and m for the first electron and k_0' and n for the second electron. The total scattering rate is given by[35]

$$\Gamma_{im}(k) = \frac{4\pi e^4 m^*}{A\hbar^3 k^3} \sum_{k_0,j.n} f_j(k_0) \int_0^{2\pi} \frac{|F_{ijmn}(q)|^2}{(q + q_{s0})^2} d\theta$$

where q_{s0} is the inverse screening length in two dimensions and $f_i(k_0)$ is the distribution function for electrons. $F_{ijmn}(q)$ is the form factor, given by

$$F_{ijmn}(q) = \int_0^\infty dz \int_{-\infty}^\infty F_i(z)\, F_j(z')\, F^*{}_m(z)\, F^*{}_m(z') \times \exp(-q|z - z'|)\, dz'$$

where $F_i(z)$ is the wave function at the ith subband. We incorporate both intra- and intersubband scattering and ignore carrier motion along the direction perpendicular to the 2D plane. Since the 2DEG is degenerate, a rejection technique accounting for the Pauli exclusion principle in the EMC modeling is adopted. During the transient phase, after the final state is selected, a random number between 0 and 1 can be used to accept or reject the transition. Screening is accounted for by a single wave-vector-independent constant. Then we introduce an ensemble of carriers, representing the photogenerated carriers injected to the 2DEG with average energies of 150 meV above the bottom of the conduction band, calculated based on electrostatic potential simulated in Figure 1c. Here only electron−electron scattering is considered since its rate is much larger than that of the electron−phonon scattering. The 2DEG density was assumed to be 5×10^{12} cm^{-2}.

Figure 4, shows the time evolution of the 2DEG energy distribution when perturbed by arrival of the optically generated

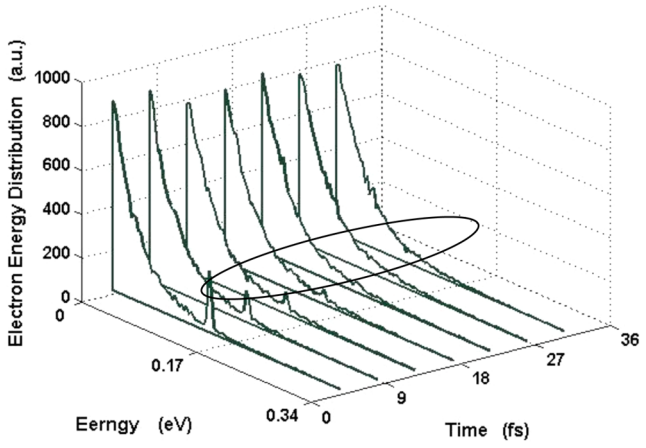

Figure 4. Time evolution of the energy distribution in 2DEG when perturbed by excess photogenerated electrons.

electrons. Each curve represents an energy distribution function at a given time, and the interval between the curves is 4.5 fs. The evolution of the nonequilibrium portion of the carriers, indicated by the solid oval in the figure, shows that these high-energy electrons reach a quasi-equilibrium with the 2DEG system in around 30 fs. The time spent by nonequilibrium carriers reaching quasi thermal equilibrium is the thermalization time, or the energy relaxation time. This femtosecond time scale is consistent with the experimental results obtained for carrier thermalization in a dense Fermi sea.[38]

An alternate formalism can be applied based on a hydrodynamic description of the response of a compressible charge layer to both harmonic perturbation and a moving charge.[39] The advantage of this analysis is that the induced charge density and scalar potential can be calculated continuously without reverting to the two-step process of drift of carriers in the absorption region and energy relaxation in the charge layer. The shortcoming is that the response is distance dependent and in the picosecond range. Hydrodynamic modeling has also successfully been applied to short-channel FETs,[21,22] which have produced tunable detectors and emitters of THz radiation[40] but are applicable to structures with lengths less than momentum relaxation distance. These studies also extend the analysis of the direct interaction of radiation with the 2D gas based on polarizability,[41] launching plasmon waves in the 2D gas, in much the same manner as performed by Allen, Tsui, and Vinter[14] for detection of infrared radiation. Incidentally, the possibility of excitation of edge magneto plasmons at room temperature in 2DEG for high-speed applications such as THz detection was predicted by von Klitzing,[42] but requires transport under a magnetic field, which as demonstrated here is not necessary in the present device.

In conclusion, electronic devices may be constructed based on the collective response of reservoirs of charge, removing a significant limitation of the operation of devices that rely on the paradigm of transport of electrons between two contacts. Not being limited by charge motion, this also removes the constraint imposed by the heavy effective mass of (slow moving) holes, since the hole reservoir reacts similarly to the electron one. The device presented here uses bilayers of electron- and hole-confined charges in a large-area (~300 μm^2/pixel) photodetector. It dissipates nanowatts of electric power, but is operable without bias, detecting as few as tens of thousands of photons at room temperature, with speeds in the hundreds of gigahertz. These properties would be expected from a device a fraction of its size if it were to be based on carrier sweep out. Besides applications to optical communications, night vision, and photovoltaics in dim light, these micro plasma devices may work as detectors of other perturbation such as charged particles or be used for direct detection of radiation such as THz. Since the reservoirs of charge can be kept near equilibrium using blocking contacts, the device can operate at room temperature.

METHODS

Device Structure and Fabrication. The layer structure and thicknesses of the MOCVD grown wafers are

material	thickness (Å)
GaAs	30
AlGaAs	564
Si delta	
AlGaAs	50
GaAs	1094
InGaAs	80
AlGaAs	50
C delta	
AlGaAs	573
GaAs	2000
GaAs SI substrate	

A second wafer with 15 pairs of GaAs/AlGaAs, which formed a Bragg mirror for 830 nm wavelength, was also grown in order to produce a resonant cavity enhanced (RCE) structure.

dx.doi.org/10.1021/ph4001229 | ACS Photonics XXXX, XXX, XXX−XXX

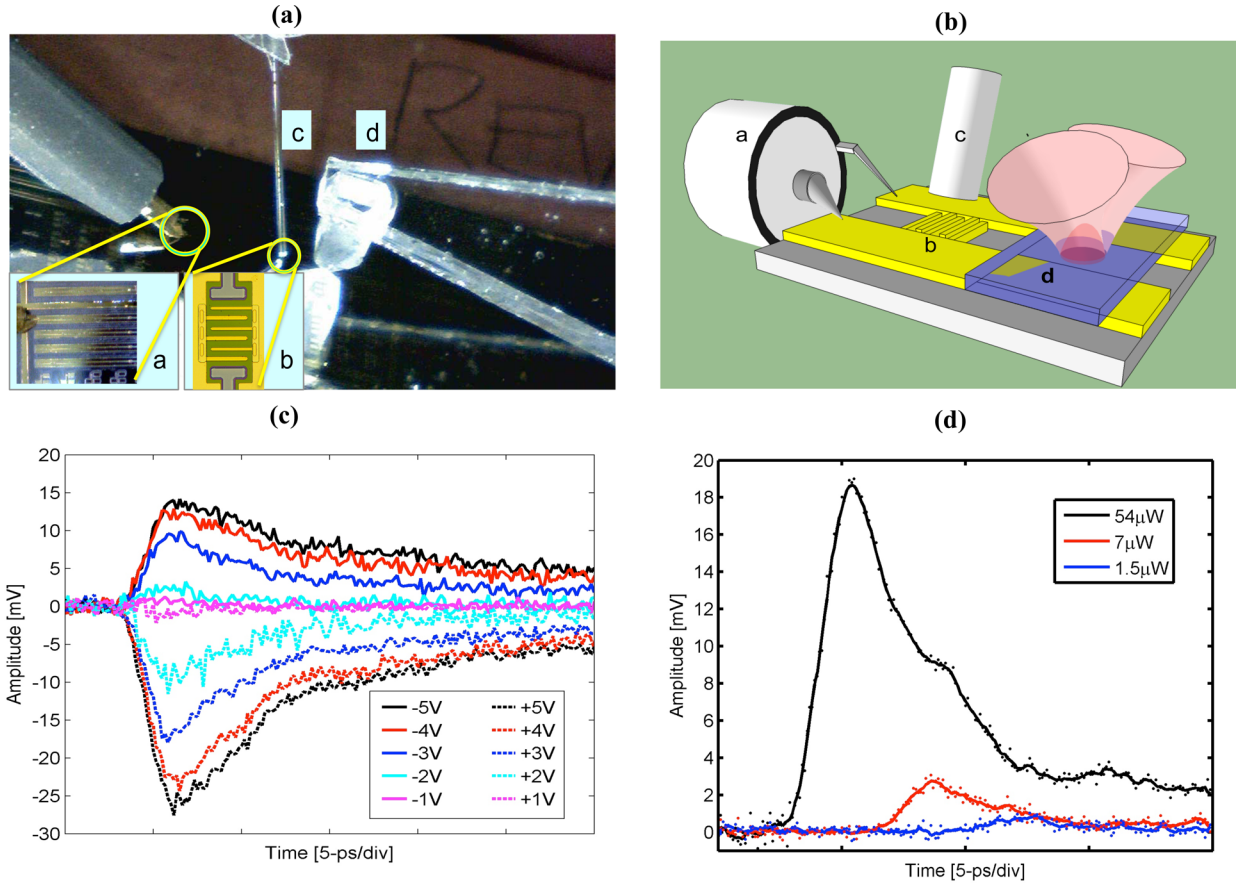

Figure 5. (a) Photo and (b) sketch of electro-optic sampling test setup showing the RF probe (a) at one end of a transmission line in the middle of which the interdigitated device is located; picture of the fabricated device under test (b); pump beam delivered by an optical fiber (c); and probe beam (d) sampled through the electro-optic crystal. (c) Time response data for bias voltage ranging from −5 to +5 V, under 7 mW optical power. (d) Time response at −2 V and 1.5, 7, and 54 μW of optical intensities.

Additionally, wafers were previously grown with (a) a delta doping layer producing 2DEG; (b) a comparison wafer without doping but the same layer structure; (c) delta doping producing a 2DHG layer; (d) comparison wafers without 2D; (e) wafers with low-temperature-grown GaAs (LT-GaAs) for buffer; (f) wafers with thin LT-GaAs; and (g) uniformly doped AlGaAs with various doping concentrations. Temporal responses of the Bragg and non-Bragg devices were similar, with the latter showing better sensitivity. Published data have shown that 2DEG wafers had fast electron response but slower fall time. 2DHG devices had a shorter tail of response compared to undoped devices.[43] LT-GaAs was fast, but up to 4 times slower than the device presented here,[44] verifying the role of the hole gas, and bilayer structure compared to unipolar traveling wave devices.

Fabrication Process.

- Contact 1 was deposited with conventional lithography, e-beam evaporation of nickel−germanium−gold−nickel−gold (50 + 300 + 600 + 300 + 2000 Å), and lift-off.
- Contact 2 was deposited with conventional lithography, recess etch, and e-beam evaporation of titanium−platinum−gold (300−300−600 Å).
- 100 nm titanium oxide was deposited by a custom-made sputtering system for passivation.
- Holes were etched after lithography and reactive ion etching with CF4 gas.
- Pads were defined by conventional lithography, e-beam evaporation of titanium−platinum−gold (300−300−3000 Å), and lift-off in an ultrasound bath.
- Devices were mesa isolated by conventional lithography and wet etching with H_2SO_4 (95−97%)/H_2O_2 (40%)/H_2O (1:8:160), T = 20 °C. Etch reached the Si substrate.

Twelve geometries of devices were fabricated with various finger widths and spacing and contact pads for signal−ground and ground−signal−ground optoelectronic measurements, as well those placed on transmission lines for electro-optic sampling measurement of the time response.

Electro-optic Sampling. Figure 5 shows the EOS measurement setup. The device under test is interdigitated with two Schottky contacts (cathode and anode), which connect to a coplanar transmission line, shown in of Figure 5a (inset). Devices with finger spacing ranging from 1.1 to 8.7 μm (and finger width in the 1−2 μm range) were fabricated in order to study the effect of transit distance. A matrix of 12 different combinations of device geometries was produced and repeated. A 40 × 40 μm^2 device area ensures that none of the devices are RC time-constant limited. Time response data were compared for the nine wafers listed above.

In essence, the EOS is an ultrafast sampling oscilloscope that uses femtosecond laser pulses to excite optoelectronic transients and then measures the electronic response by probing the refractive index change of an electro-optic crystal placed on top of the device and/or transmission line. In our setup the laser is split

dx.doi.org/10.1021/ph4001229 | ACS Photonics XXXX, XXX, XXX−XXX

into two paths: one coupled into a fiber (labeled c in Figure 5a,b) to excite the device (labeled b in Figures 5a,b) and another path that passes through a $LiTaO_3$ crystal (labeled d in Figure 5a,b) to sample the electric field of the propagating response. By varying the optical path of the sampling beam, the temporal response of the device is observed with a time resolution limited by the laser pulse width and the response of the electro-optic crystal. Our amplitude sensitivity is limited by the noise in our detection system. To increase the sensitivity to sub-mV levels, we modulated the switching beam at 80 kHz and performed phase-sensitive detection with a lock-in amplifier on the light analyzed (with a polarizer and differential detection) from the $LiTaO_3$ crystal. In this experiment ~100 fs pulses from a Ti:sapphire laser with a center wavelength of 830 nm were split into the two paths. The path that is coupled into a fiber to excite the device under test (DUT) (labeled c in Figure 5a,b) is dispersed by the fiber and exits as a 400 fs chirped optical pulse. The second laser path that passes through the $LiTaO_3$ crystal (Figure 5a,d) to sample the propagating electric field broadens slightly to a 150 fs optical pulse at the crystal. The photodetector's electronic response is coupled to a coplanar strip transmission line. The separation from the fiber exciting the device to the optical sampling crystal is 250 μm. The CPS transmission line is contacted with microwave probes (labeled "a" in Figure 5a,b) for dc bias and <50 GHz measurements. Bias values from −15 to +15 V were applied to the MSM structure with average optical powers ranging from 250 nW to 10 mW.

Figure 5c shows the response of a device with a 1.1 μm finger spacing, under 7 μW average optical power, for a bias voltage range of ±5 V. As reported in Figure 3a, the device is fastest with low or no applied bias since at higher bias values the charge reservoirs empty, and the electric field component perpendicular to the contacts weakens relative to the tangential field of the applied bias voltages. This causes a longer transit distance and higher loss in the 2D degrading device response. Data were taken for various geometries and with spatial localization of the light beam. Device response was not dependent on the excitation beam's proximity to either cathode or anode and, as Figure 3c shows, was independent of the distance between them. The device responds to optical excitation at zero applied bias as seen in Figure 3a. The device response at −2 V applied bias, but under different optical intensities, is shown in Figure 5d.

Pulses with as low as 250 nW were detected with an electronic pulse width less than 4 ps. Increasing the optical intensity widens the temporal response. This is expected since the separation of electron hole pairs produces an electric field in the vertical direction that counters the built-in field between the 2D reservoirs. Further saturation effects are expected if the EHP densities become comparable to 2DEG and 2DHG densities, forcing the system out of the perturbation regime. Incidentally, the delay in electric response observed in this figure is due to photon travel in the neutral density filters which are used to attenuate power; that is, EOS is measuring the travel time through the optical filters as well.

Components of Total Temporal Response. Several factors are involved in the temporal response measured via electro-optic sampling. The overall response comprises three major elements: (1) the device response, (2) the signal propagation, and (3) the electro-optic sampling system measurement. We measure the combination of these responses, resulting in a measured signal that is distorted and often results in a measured transient with a slower temporal response than the device's intrinsic speed. Our device dimensions are a fraction of the electrical transient's propagation velocity of 130 μm/ps, allowing for potential temporal broadening on that time scale.

The transmission line adds attenuation and dispersion as the device's signal travels toward the electro-optic detection point. The transmission line's characteristics can be calculated, however, at frequencies exceeding 50−100 GHz; care must be taken to ensure the accuracy of calculations. Finally, the electro-optic sampling system has its own intrinsic response based upon parameters such as optical pulse width, optical and electrical transit times in the crystal, and optical beam size. In this experiment, our EOS system has a 400 fs switching pulse and a 150 fs sampling pulse. Since the EO crystal is thin (~50 μm), the system is primarily limited by the optical pulse widths. As a case in point, the convolution of a 1500 and 400 fs Gaussian pulse (fwhm) produces a 427 fs Gaussian pulse response. This laser system response was applied to measure three waveforms: (1) unit step function, (2) unit step function multiplied by an exponential decay, and (3) a 2 ps wide Gaussian pulse. The convolution of the laser system response with these waveforms results in 0.46 ps broadened rise times and up to 0.5 ps broadened pulse widths.

Reflection Timing. The device under test is located in the center of a transmission line of length $2z_1$. The EO crystal is located a distance z_0 from the MSM. The reflection from the nonterminated transmission line, R_1, is a distance of $z_1 - z_0$, while the reflection from the transmission line with the high-speed/voltage-bias probe, R_2, is on the other side of the MSM and therefore a distance $z_1 + z_0$. R_1 is positive (open circuit), while R_2 is minimal due to impedance matching with the high-speed probe. The arrival times of the DUT's pulse and its reflections from the transmission line ends are as follows: pulse: $t_0 = z_0 = c'$; first reflection (R_1): $t_{R1} = 2(z_1 - z_0)/c' + t_0$; second reflection ($R_2$): $t_{R2} = 2_{z1}/c' + t_0$.

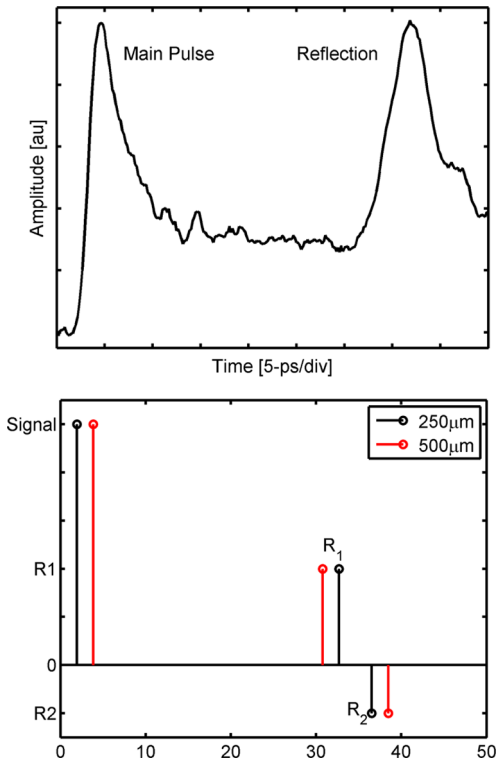

Figure 6. (Top) Measurements showing pulse and its reflection. (Bottom) Pulse delay times and reflections for distances of 250 and 500 mm between the device and probe on the transmission line.

dx.doi.org/10.1021/ph4001229 | ACS Photonics XXXX, XXX, XXX−XXX

Assuming the propagation velocity, c', on the 4.5 mm transmission line is approximately 130 μm/ps ($c' = c_0/2.3$), then the pulse delay times for an EO crystal a location 250 and 500 μm from the MSM is shown graphically in Figure 6. Using this information, we can analyze the pulsed response data also shown in Figure 6. Here the main pulse is observed with a sharp rise time and is measured ~250 μm from the MSM followed by the reflection of this pulse from the transmission line approximately 30 ps later. Since the pulse travel distance is known, we can calculate an average propagation velocity on the transmission line of 130 μm/ps (using the midpoint of each pulse's rise time). These data provide an approximate pulse broadening over the 250 μm from the DUT of <0.3 ps. In summary, while the intrinsic device response is not measured, the analysis of the transmission line dispersion and the EOS system response demonstrates that the extrinsic device response may be as much as 0.4 ps shorter than the measured data.

AUTHOR INFORMATION

Corresponding Author

*E-mail: nabet@ece.drexel.edu. Tel: +1.215.895.6761.

Author Contributions

$^{\perp}$F. Quaranta and A. Cola contributed equally to this work.

Notes

The authors declare no competing financial interest.

ACKNOWLEDGMENTS

This work was partially supported by NSF Award No. ECCS-0702716, the Office of Naval Research, ASEE-ONR Summer Faculty Research Fellowship, and Italian CNR Short Term Mobility grants.

REFERENCES

(1) Lilienfeld, J. E. Device for Controlling Electric Current. U.S. Patent 1,900,018. 1933.

(2) Brattain, W. H.; Bardeen, J. Surface Properties of Germanium. *Bell Syst. Technol. J.* **1953**, *32*, 1−41.

(3) Haug, H.; Koch, S. W. *Quantum Theory of the Optical and Electronic Properties of Semiconductors*, 5th ed.; World Scientific: Singapore, 2009.

(4) Tonks, L.; Langmuir, I. Oscillations in Ionized Gases. *Phys. Rev.* **1929**, *33*, 195−210.

(5) Debye, P.; Hückel, E. Zur Theorie der Elektrolyte. I. Gefrierpunktserniedrigung und Verwandte Erscheinungen [The Theory of Electrolytes. I. Lowering of Freezing Point and Related Phenomena]. *Phys. Z.* **1923**, *24*, 185−206 as reported in Fetter, A. L.; Walecka, J. D. *Quantum Theory of Many Particle System*; McGraw-Hill: New York, 1971; Sections 3 and 14.

(6) Bohm, D.; Pines, D. A. Collective Description of Electron Interactions: III. Coulomb Interactions in a Degenerate Electron Gas. *Phys. Rev.* **1953**, *92*, 609−625.

(7) Gabor, D. Collective Oscillations and Characteristic Electron Energy Losses. *Philos. Mag.* **1956**, *1*, 1−18.

(8) Landau, L. D.; Lifshitz, E. M. *Electrodynamics of Continuous Media*; Addison-Wesley: Reading, MA, 1960.

(9) Ritchie, R. H. Plasma Losses by Fast Electrons in Thin Films. *Phys. Rev.* **1957**, *106*, 874−881.

(10) Wilberg, E.; Ingelsfield, J. E. Collective Modes and Ground State Energy of the Semi-Infinite Electron Gas. *Phys. Rev.* **1960**, *188*, 640−643.

(11) Ando, T.; Fowler, A. B.; Stern, F. Electronic Properties of Two-Dimensional Systems. *Rev. Mod. Phys.* **1982**, *54*, 437−672.

(12) Allen, S. J.; Tsui, D. C.; Logan, R. A. Observation of the Two-Dimensional Plasmon in Silicon Inversion Layers. *Phys. Rev. Lett.* **1977**, *38*, 980−983.

(13) Grimes, C. C.; Adams, G. Observation of Two Dimensional Plasmons and Electron-Ripplon Scattering in a Sheet of Electrons on Liquid Helium. *Phys. Rev. Lett.* **1976**, *36*, 145−148.

(14) Allen, S. J.; Tsui, D. C.; Vinter, B. On the Absorption of Infrared Radiation by Electrons in Semiconductor Inversion Layers. *Solid State Commun.* **1976**, *20*, 425−428.

(15) Dingle, R.; Stormer, H. L.; Gossard, A.; Wiegmann, W. Electron Mobilities in Modulation-Doped Semiconductor Heterojunction Superlattices. *Appl. Phys. Lett.* **1978**, *33*, 665−667.

(16) Von Klitzing, K.; Englert, T.; Fritzsche, D. Transport Measurements on InP Inversion Metal-Oxide Semiconductor Transistors. *J. Appl. Phys.* **1980**, *51*, 5893−5897.

(17) Mimura, T.; Hiyamizu, S.; Fujii, T.; Nanbu, K. A New Field-Effect Transistor with Selectively Doped GaAs/AlxGa1-x As Heterojunctions. *Jpn. J. Appl. Phys.* **1980**, *19*, L225−L227.

(18) Mimura, T. The Early History of the High Electron Mobility Transistor (HEMT). *IEEE Trans. Microwave Theory Tech.* **2002**, *50*, 780−782.

(19) Delagebeaudeuf, D.; Delescluse, P.; Etienne, P.; Laviron, M.; Chaplart, J.; Linh, N. T. Two-Dimensional Electron Gas MESFET Structure. *Electron. Lett.* **1980**, *16*, 667−668.

(20) Deal, W.; Mei, X. B.; Leong, M. K. H.; Radisic, V.; Sarkozy, S.; Lai, R. THz Monolithic Integrated Circuits Using InP High Electron Mobility Transistors. *IEEE Trans. Terahertz Sci. Technol.* **2011**, *1*, 25−33.

(21) Dyakonov, M. I.; Shur, M. S. Shallow Water Analogy for a Ballistic Field Effect Transistor: New Mechanism of Plasma Wave Generation by dc Current. *Phys. Rev. Lett.* **1993**, *71*, 2465−2468.

(22) Dyakonov, M. I.; Shur, M. S. Plasma Wave Electronics: Novel Terahertz Devices Using Two Dimensional Electron Fluid. *IEEE Trans. Electron Devices* **1996**, *43*, 1640−1645.

(23) Sze, S. M.; Coleman, D. J.; Loya, A. Current Transport in Metal−Semiconductor−Metal MSM Structures. *Solid-State Electron.* **1971**, *14*, 1209−1218.

(24) Bowers, J. E.; Burrus, C. A. High-Speed Zero-Bias Waveguide Photodetectors. *Electron. Lett.* **1986**, *22*, 905−906.

(25) Kato, K. Ultrawide-Band/High-Frequency Photodetectors. *IEEE Trans. Microwave Theory Tech.* **1999**, *80*, 1265−1275.

(26) Dianat, P.; Prusak, R.; Cola, A.; Quaranta, F.; Nabet, B. An Unconventional Hybrid Variable Capacitor with a Two-Dimensional Electron System. *IEEE Trans. Electron Devices* **2014**, *61*, 445−451.

(27) Ryzhii, V.; Ryzhii, M.; Mitin, V.; Shur, M. S.; Satou, A.; Otsuji, T. Terahertz Photomixing Using Plasma Resonances in Double-Graphene Layer Structures. *J. Appl. Phys.* **2013**, *113* (174506), 1−7.

(28) Keldysh, L. V.; Kozlov, A. N. *Zh. Eksp. Teor. Fiz.* **1968**, *54*, 978−986; Collective Properties of Excitons in Semiconductors. *Sov. Phys. JETP* **1968**, *27*, 521−528.

(29) Joglekar, Y. N.; Balatsky, A. V.; Das Sarma, S. Wigner Supersolid of Excitons in Electron-Hole Bilayers. *Phys. Rev. B* **2007**, *74* (233302), 1−4.

(30) Sivan, U.; Solomon, P. M.; Shtrikman, H. Coupled Electron-Hole Transport. *Phys. Rev. Lett.* **1992**, *68*, 1196−1198.

(31) Pohlt, M.; Lynass, M.; Lok, J. G. S.; Dietsche, W.; Klitzing, K.v.; Eberl, K.; Muhle, R. Closely Spaced and Separately Contacted Two-Dimensional Electron and Hole Gases by In Situ Focused-Ion Implantation. *Appl. Phys. Lett.* **2002**, *80*, 2105−2107.

(32) Anwar, A.; Nabet, B. Barrier Enhancement Mechanisms in Heterodimensional Contacts and Their Effect on Current Transport. *IEEE Trans. Microwave Theory Tech.* **2002**, *50*, 68−71.

(33) Shockley, W. Currents to Conductors Induced by a Moving Point Charge. *J. Appl. Phys.* **1938**, *9*, 635−636.

(34) Ramo, S. Currents Induced by Electron Motion. *Proc. I.R.E* **1939**, *27* (9), 584−585.

(35) Zhao, X. *Carrier Transport in High Speed Photodetectors Based on Two-Dimensional Gas*, Ph.D. Dissertation, Drexel University, 2006, Chapter 5.

(36) Atwater, H.; Polman, A. Plasmonics for Improved Photovoltaic Devices. *Nat. Mater.* **2010**, *9*, 205−213.

(37) Jacoboni, C.; Reggiani, L. The Monte Carlo Method for the Solution of Charge Transport in Semiconductors with Applications to Covalent Materials. *Rev. Mod. Phys.* **1983**, *55*, 645−705.
(38) Knox, W.; Chemla, D.; Livescu, G.; Henry, J. E. Femtosecond Carrier Thermalization in Dense Fermi Seas. *Phys. Rev. Lett.* **1988**, *61*, 1290−1293.
(39) Fetter, A. L. Electrodynamics of a Layered Electron Gas. I. Single Layer. *Ann. Phys.* **1973**, *81*, 367−393.
(40) Ryzhii, V.; Sato, A.; Otsuji, T.; Shur, M. S. Plasma Mechanisms of Resonant Terahertz Detection in a Two-Dimensional Electron Channel with Split Gates. *J. Appl. Phys.* **2008**, *103* (014504), 1−6.
(41) Stern, F. Polarizability of a Two-Dimensional Electron Gas. *Phys. Rev. Lett.* **1967**, *18*, 546−548.
(42) von Klitzing, K.; Mikhailov, K. S.; Smet, J. H.; Kukushkin, I. V. A Detector for Electromagnetic Radiation and a Method of Detecting Electromagnetic Radiation, U.S. Patent 6,987,484, 2006.
(43) Zhao, X.; Gallo, E. M.; Cola, A.; Quaranta, F.; Currie, M.; Spanier, J. E.; Nabet, B. Time Response of Two-Dimensional Gas-Based Vertical Field Metal−Semiconductor−Metal Photodetectors. *IEEE Trans. Electron Devices* **2008**, *55*, 1762−1770.
(44) Currie, M.; Quaranta, F.; Cola, A.; Gallo, E. M.; Nabet, B. Low-Temperature Grown GaAs Heterojunction Metal-Semiconductor-Metal Photodetectors Improve Speed and Efficiency. *Appl. Phys. Lett.* **2011**, *99* (203502), 1−3.